

**Norwegian University of Science and
Technology
NTNU**

Department of Chemical Engineering

Associate Prof. Johannes Jäschke

**Modeling a Multiphase
Subsea Separation System**

TKP 4550 Specialization Project

by

Torstein Bishop

Co-supervisor: Tamal Das

Trondheim, December 18, 2015

Abstract

The aim of this project has been to make the models for the liquid-liquid separation system, proposed by Tyvold in his Master thesis, compatible for oil-gas separation with respect to control purposes, by using parameters Fahad used in his Master thesis. The model is therefore required to be accurate while relative simple to reduce computational costs.

The separator studied in this project is a deliquidizer that receives a gas-rich stream and purifies it by separating out the oil-residue. The deliquidizer has been tested towards experimental data obtained from industry and analysed towards varying flow rates and flow split.

The model for the deliquidizer showed satisfying results for the gas volume fraction when compared towards the experimental data, however, it seemed to overestimate the liquid volume fractions. The performance of the separator when tested towards varying flow rates showed expected results. When testing the model towards varying flow splits, the performance showed results as expected with high flow splits (Flow split > 0.5), but seemed to deviate from what was expected at low flow splits. Investigations into the reasons behind these deviations has not been in the scope of the project and will be conducted in future work.

The models for the deliquidizer were implemented into MATLAB and all simulations were conducted by using the same program.

Preface

This report was written as a part of the course TKP 4550 Specialization Project during autumn 2015 in the fifth year of the chemical engineering degree at the Norwegian University of Science and Technology.

I would like to thank my supervisor Associate Professor Johannes Jäschke for guidance, advice and valuable discussions during my work. A thank you is also on order for Ph.D Candidate Tamal Das for help and advice during the semester as well as valuable feedback during when writing this report.

I am grateful to all my friends for giving me great procrastination opportunities through frequent coffee breaks, lunches and irrelevant discussions in the office.

Contents

Abstract	i
Preface	i
List of Figures	iv
List of Symbols	vi
List of Acronyms	ix
1 Introduction	1
1.1 Purpose of project	2
2 Theory	3
2.1 Sedimentation	3
2.2 Coalescence	4
2.3 Diffusion	6
2.4 Swirl Element	7
2.5 Separation Efficiency	8
3 Description of Model	10
3.1 Overall Model	10
3.2 Deliquidizer	11
3.2.1 Axial Velocity	12
3.2.2 Tangential Velocity	13
3.2.3 Radial Velocity	16
3.2.4 Droplet size	17
3.2.5 Equation of Motion	18

3.2.6	Re-Entrainment	20
3.2.7	Soave-Redlich-Kwong Equation of State	22
3.2.8	Viscosity of mixtures	24
3.3	Model input	26
3.3.1	Separator dimensions	27
3.3.2	Empirical Parameters	28
3.3.3	Fluid Properties	29
4	Results & Discussion	30
4.1	Model vs Experimental data	30
4.2	Flow rate effect	33
4.3	Flow split effect	35
5	Conclusion	38
5.1	Further Work	39
A	MATLAB-scripts	43
A.1	Main Function	43
A.2	Separator Performance Function	49
A.3	The Governing Equations	50
A.4	Composition Calculations	52
A.5	Soave-Redlich-Kwong Equation of State	54
A.6	Fourth Order Runge-Kutta	57
A.7	Shooting Method	58
B	Experimental data	61
C	Separator profiles	64

List of Figures

2.1	a) Two droplets melt together to one larger droplet. b) A droplet melts together with the bulk phase. Figure adapted from Tyvold [15].	6
2.2	An illustration of the swirl element, where the flow is from the left to the right. The vortex is induced by the vanes that have an angle θ to the axial direction. Figure from Tyvold [15].	8
3.1	Flow diagram for the overall model consisting of the three separators. Figure from Tyvold [15].	11
3.2	Velocity profile in the separator illustrating the velocity differences between the regions. Figure adapted from Tyvold [15].	13
3.3	Profile of the tangential velocity, v_θ , for a Rankine vortex with inside a separator with radius R. Figure adapted from Tyvold [15].	14
3.4	Left: Streamlines (blue) according to the model with no net flow across boundary, the pressure is lower at the LPO than in the HPO. Right: Streamlines with the re-entrainment concept included and a flow going inwards. Figure from Tyvold [15].	21
3.5	Illustration of the viscosity profile in an oil-water emulsion as a function of the water cut, wc , and the dashed line marks the phase inversion. Figure from Tyvold [15].	25

3.6 Illustration of the viscosity profile in this project as a function of the gas volume fraction, GVF, where μ_o is the viscosity of the oil and μ_g is the viscosity of the gas. The dashed line marks the phase inversion. 26

4.1 Deliquidizer performance with inlet gas fraction of 0.8 and flow split of 0.8 as a function of inlet flow rate, q_{in} 33

4.2 Deliquidizer performance with inlet gas fraction of 0.8 and flow rate of $140 \text{ m}^3/h$ as a function of flow split, FS 36

B.1 Time dependent experimental data for the outflows through the light phase outlet (LPO) and the heavy phase outlet (HPO). 61

B.2 Time dependent experimental data for the gas volume fraction (GVF) in the light phase outlet (LPO) and liquid volume fraction (LVF) in the heavy phase outlet (HPO) obtained from the industry. 62

B.3 Data for how much the liquid boot is filled, given in percent, towards the hours of operation. 63

C.1 Residence time in the separator, τ , as a function of inlet flow rate, q_{in} , with a flow split of $FS = 0.8$ and inlet gas fraction of $\alpha_{in} = 0.8$ 64

C.2 Droplet size in the separator as a function of inlet flow rate, q_{in} , with a flow split of $FS = 0.8$ and inlet gas fraction of $\alpha_{in} = 0.8$ 65

List of Symbols

Latin letters

Symbol	Description	Unit
a_c	Centrifugal acceleration	m s^{-2}
C	Concentration	mol m^{-3}
c	Droplet size correlation intercept	m
D_d	Droplet diameter	m
C_{decay}	Decay factor for decreased vortex momentum	-
D_{diff}	Diffusion coefficient	$\text{m}^2 \text{s}^{-1}$
D_{sep}	Separator diameter	m
E_A	Attractive energy between two droplets	J
E_R	Repulsive energy between two droplets	J
E_T	Total interaction energy between two droplets	J
F_d	Gravitational buoyancy force	N
F_r	Frictional force	N
FS	Flow split	-
f	Frictional coefficient	kg s^{-1}
GR	Gas recovery	-
g	Gravitational acceleration	m s^{-2}
k_{re-en}	Re-entrainment proportionality constant	m^2
L	Separator length	m
M_m	Molar mass	kg mole^{-1}
m	Droplet size correlation slope	h m^{-2}

Symbol	Description	Unit
p	Pressure	Pa
p_c	Critical pressure	Pa
q_{HPO}	Flow rate through heavy phase outlet	$\text{m}^3 \text{s}^{-1}$
q_{in}	Inlet flow rate	$\text{m}^3 \text{s}^{-1}$
q_{LPO}	Flow rate through light phase outlet	$\text{m}^3 \text{s}^{-1}$
q_{re-en}	Re-entrainment flow rate	$\text{m}^3 \text{s}^{-1}$
R	Separator radius	m
R_c	Radius of vortex core with solid body rotation	m
R_{gc}	Universal gas constant	$\text{J mole}^{-1} \text{K}^{-1}$
R_i	Radius of gas-extraction pipe	m
r	Radial coordinate	m
r_d	Droplet radius	m
r_{in}	Radial position fro droplet at inlet	m
T	Temperature	K
T_c	Critical temperature	K
T_r	Reduced temperature	-
V_d	Volume of particle	m^3
V_m	Molar volume	$\text{m}^3 \text{mole}$
v	Velocity	m s^{-1}
v_r	Radial velocity	m s^{-1}
v_{θ}^{max}	Maximum tangential velocity	m s^{-1}
v_{θ}^0	Initial tangential velocity	m s^{-1}
v_{θ}	Tangential velocity	m s^{-1}
v_z	Axial velocity	m s^{-1}
v_{θ}	Tangential velocity	m s^{-1}
t	Time	s
x	Spatial coordinate	m
Z	Compressibility factor	-
z	Spatial coordinate	m

Greek letters

Symbol	Description	Unit
α_{HPO}	Gas volume fraction in heavy phase outlet	-
α_{in}	Inlet gas volume fraction	-
α_{LPO}	Gas volume fraction in light phase outlet	-
$\alpha'_{o,HPO}$	Liquid fraction in HPO before re-entrainment	-
$\alpha'_{o,LPO}$	Liquid fraction in LPO before re-entrainment	-
$\alpha_{o,HPO}$	Liquid fraction in HPO after re-entrainment	-
$\alpha_{o,LPO}$	Liquid fraction in LPO after re-entrainment	-
β	Smoothing parameter	-
Δ	Difference in the variables that follows	-
η_{Split}	Split efficiency	-
μ	Viscosity	Pa s
μ_g	Viscosity of gas	Pa s
μ_o	Viscosity of oil	Pa s
Ω	Swirl number	-
ω	Acentric factor	-
π	Ratio of a circles circumference to diameter	-
ρ	Density	kg m ⁻³
ρ_c	Density of continuous phase	kg m ⁻³
ρ_d	Droplet density	kg m ⁻³
σ	Interfacial tension	N m ⁻²
τ	Residence time	s
θ	Angular coordinate	rad
θ_v	Angle of vanes on swirl element to z-direction	rad

List of Acronyms

Acronym	Description
GVF	Gas volume fraction
HPO	Heavy phase outlet
LPO	Light phase outlet
LVF	Liquid volume fraction
wc	Water cut/ water volume fraction

1 Introduction

With sinking oil prices, more environmentally friendly operations and less accessible oil and gas fields the demand for innovative thinking and new technology is increasing. One of these new technologies that can help overcome the current difficulties is subsea separation. Subsea separation offer reduced topside facility costs, environmentally friendly operations, increased production and recovery [5]. By reducing topside and operational costs the economical lifetime of the asset is increased, which will result in increased recovery. Subsea systems make it possible to have viable production from small fields that can be tied together and fed back to a host facility for processing. In addition it also gives the possibility of production from remote fields and especially in deep water [14].

Even though there are a lot of benefits by using subsea separation there are also downsides, issues and challenges regarding the technology. Due to the depths where the subsea systems are placed, the accessibility of the separators are reduced resulting in difficulties in maintenance and retrieval of the modules [14]. The dimensions of the compact separator are smaller than the conventional separators, resulting in reduced residence times. The reduction in the residence time can lead to control issues since the control valve must respond a lot faster to any disturbances in order to keep the separator at its operating set-point [10].

To overcome the control issues, which will enable safe and profitable operations, optimization becomes vital in order to operate the separator at its optimal conditions [15]. In order to optimize the system simple models giving low computational cost, which yield accurate results are vital.

1.1 Purpose of project

The purpose of the project is to make the models for the liquid-liquid system in the Master thesis by Tyvold [15] compatible for a liquid-gas separation. The modeled separator in this project will be a deliquidizer which will receive a gas-rich stream and separate out the oil remains in the flow. The models from the Master thesis are based on first principles thus containing few empirical parameters and correlations. These parameters have been taken from Matovu's Master thesis [8] in order to combine the empirical parameters from his gas-liquid system to the models from Tyvold's work.

2 Theory

In this chapter the basic theory for the separation process is presented. The main phenomena effecting separation are sedimentation, coalescence and diffusion and they are presented in sections 2.1, 2.2 and 2.3 respectively. The swirl element and its fundamentals are presented in section 2.4 while the measurements used to evaluate the separation performance are presented in section 2.5.

2.1 Sedimentation

Dispersed phase droplets in a colloidal dispersion that have a density that differs from the density of the continuous phase will induce sedimentation or creaming due to gravitational forces. The rate at which the particles will sediment are mainly given by the size and density of the particle. A particle with density ρ_d and volume V_d , in a continuous phase with density ρ_c will be exposed to the gravitational buoyancy force, F_d , given by the following equation [9]:

$$F_d = V_d(\rho_d - \rho_c)g \quad (2.1)$$

g is in this case the gravitational acceleration and the main driving force behind the sedimentation process. If $F_d > 0$ the particle will sink as sedimentation occurs and if $F_d < 0$ the particle rises and creaming occurs. The motion of particles will retard due to the frictional force F_r caused by the viscosity of the continuous phase. Initially the velocity of the droplets will increase rapidly, but since the force, F_r is proportional to the velocity,

v , the particle will nearly instantaneously reach its terminal velocity [9]. The frictional force can be expressed by [9]:

$$F_r = f \left(\frac{dx}{dt} \right) = f v \quad (2.2)$$

The proportionality constant f is often referred to as the frictional coefficient. This coefficient can be described by hydrodynamic theories [9], but due to its complexity it is often approximated by Stokes' law, and if Stokes' law is assumed to be valid, f can be expressed by [9]:

$$f = 6\pi\mu r_d \quad (2.3)$$

where μ is the viscosity of the continuous phase and r_d is the particle radius. When the particle reaches its terminal velocity the gravitational buoyancy force equals the frictional force. By inserting equation 2.3 into 2.2 and equating equation 2.1 and 2.2, the terminal velocity of a particle can be expressed by:

$$v = \frac{2r_d^2(\rho_d - \rho_c)g}{9\mu} \quad (2.4)$$

2.2 Coalescence

Coalescence is a phenomena that is necessary in order for separation of the phases to occur. Inside the separator coalescence will occur in two forms. The first being when two droplets merge together into one droplet, see Figure 2.1 a), and second being when droplets combine with the continuous phase through the bulk interface, see Figure 2.1 b). The first form occurs

due to the droplets having different velocities caused by diffusion and turbulence [15]. This will cause collisions, which may lead to coalescence if the total interaction energy, E_T , is sufficiently low and the kinetic energy is sufficiently large. The total interaction energy is the sum of the attractive, E_A , and repulsive energy, E_R , between the droplets and can be expressed as [9]:

$$E_T = E_A + E_R \quad (2.5)$$

The droplet size will increase due to coalescence thus increasing separation through sedimentation. The second form of coalescence is a vital part in order to separate the two phases. Coalescence of droplets through the bulk interface can be rate determining for the separation process in cases where the interfacial tension is high. In these cases droplets will accumulate close to the bulk interface [15].

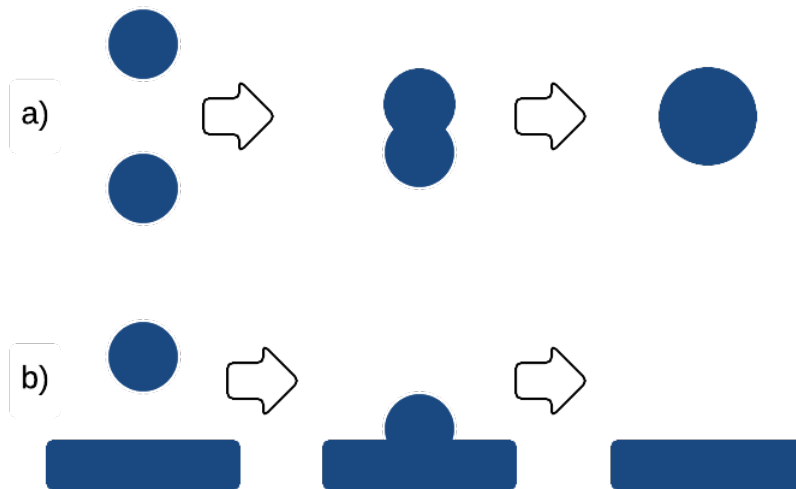


Figure 2.1: **a)** Two droplets melt together to one larger droplet. **b)** A droplet melts together with the bulk phase. Figure adapted from Tyvold [15].

2.3 Diffusion

Diffusion is a process that is driven by concentration differences, where particles travel from an area of high concentration to an area of low concentration due to Brownian motions. When sedimentation occurs, concentration gradients will develop, which will trigger diffusion and try to counteract the sedimentation and thereby also the separation process. The diffusion of a particle with a concentration gradient in x-direction is expressed by Fick's law in the following equation [9]:

$$\frac{dC}{dt} = D_{diff} \frac{\partial^2 C}{\partial x^2} \quad (2.6)$$

where D_{diff} is the diffusion constant for the system and C is the concentration of the dispersed phase. In this project it is, however, assumed that the force driving the sedimentation has such a high magnitude that the sedimentation velocity is greater than the diffusion velocity leading to a negligible effect of diffusion on the overall separation process.

2.4 Swirl Element

The model developed by Tyvold [15] contains a static swirl element that generates a vortex inside the separator. The vortex inside the separator will introduce centrifugal forces on the particles and thus lead to sedimentation of the particles [15, 16]. According to van Campen [16], the velocity downstream of the swirl element will have two profiles, one axial and one tangential, where a relationship between them is given by:

$$\tan \theta_v = \frac{v_\theta}{v_z} \quad (2.7)$$

Here v_z is the axial velocity at the end of the vanes, v_θ is the tangential velocity at the same location while θ_v is the angle of the vanes to the axial direction. An illustration is shown in Figure 2.2.

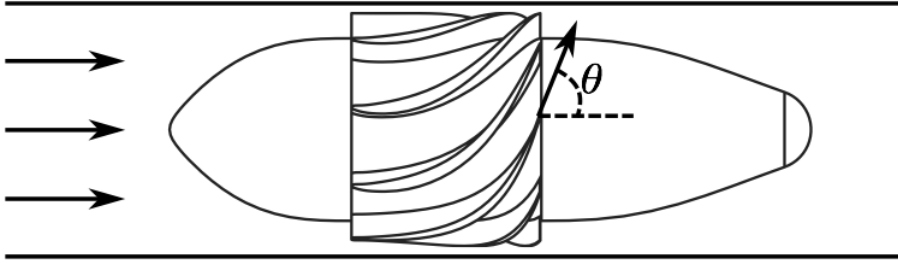


Figure 2.2: An illustration of the swirl element, where the flow is from the left to the right. The vortex is induced by the vanes that have an angle θ to the axial direction. Figure from Tyvold [15].

2.5 Separation Efficiency

Tyvold defined two sets of measures in order to evaluate the efficiency and performance of the separator. The measures of efficiency are the dilute and dispersed efficiency [15]. The efficiencies will be used in this project, however with different names that make more sense for a gas-liquid system. The dilute efficiency will in this case be gas recovery and is defined as [15]:

$$GR = \frac{\alpha_{LPO} q_{LPO}}{\alpha_{in} q_{in}} \quad (2.8)$$

Where α_{LPO} and q_{LPO} are the gas volume fraction and volumetric flow in the Light Phase Outlet (LPO) and α_{in} and q_{in} are the gas volume fraction and the volumetric flow into the separator. The gas recovery is the fraction of gas that is kept in the LPO and from equation 2.8 it is clear that the gas recovery is one if there is no gas in the Heavy Phase Outlet (HPO) and zero if there is no gas in the LPO [15].

The dispersed efficiency will in this project be called the split efficiency and is defined as:

$$\eta_{Split} = 1 - \frac{(1 - \alpha_{LPO}) q_{LPO} + \alpha_{HPO} q_{HPO}}{q_{in}} \quad (2.9)$$

The split efficiency is a measure of the amount of liquid that exits through the desired outlet and from equation 2.9 it is clear that the efficiency is one if the HPO is pure liquid and the LPO is pure gas [15].

3 Description of Model

In this chapter the model for the separator is presented with the assumptions made while building these models. The models used are primarily the models Tyvold [15] developed in his Master thesis and are complemented by using the models Matovu [8] used in his Master thesis when needed. The parameters needed in this project are primarily taken from Matovu [8].

Section 3.1 presents and gives a brief introduction to the model generated by Tyvold [15], which this project will be building on in order to make it compatible with gas-liquid separation. In section 3.2 the models for the deliquidizer are presented while section 3.3 presents the parameters needed as input to the model.

3.1 Overall Model

Tyvold presented in his Master Thesis an overall flowsheet for the subsea separation system, see Figure 3.1, which consists of three separators; one gravity and two swirl separators. The gravity separator performs a bulk separation of the fluid from the well while the the deoiler and dewaterer purifies the water-rich and oil-rich streams, respectively [15].

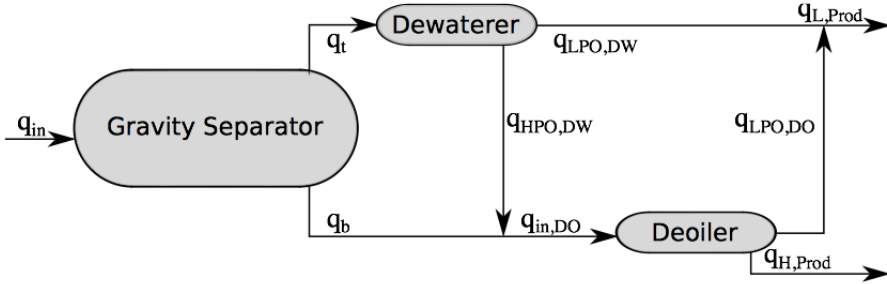


Figure 3.1: Flow diagram for the overall model consisting of the three separators. Figure from Tyvold [15].

The purpose of this project is to make the models from Tyvold [15] compatible for gas-liquid separation, so in this project the flow diagram will be somewhat different compared to the one presented in Figure 3.1. The dewaterer in this case will be a deliquidizer and the deoiler will be a degasser. In this project the focus has been on models for the separation process in the deliquidizer and these models are presented in section 3.2.

3.2 Deliquidizer

Even though the system in this project is gas-liquid compared to the liquid-liquid system that was presented by Tyvold [15], the models used in this project are based on the models for the liquid-liquid system.

The model for the separation process inside the swirl separator is based on centrifugal forces acting on the oil droplets due to the co-current swirl generated by the swirl element. The oil droplets are represented by the average droplet size [15]. The inlet stream will pass through the swirl element which will induce a vortex in the flow that will flow through the

separator. The centrifugal forces on the oil droplets, generated by the vortex, will force the droplets outward towards the separator walls due to the difference in density between the oil droplets and the continuous gas phase. At the end of the separator there is a gas-extraction pipe, with radius $R_i < R$, where the light phase is extracted. The flow outside R_i will flow past the gas-extraction pipe and exit through the heavy phase outlet [8, 15].

3.2.1 Axial Velocity

By using valves on either of the outlet streams, the flow split (FS) and the flow rates in the outlet streams can be manipulated. The flow split can be defined as the ratio between the light phase outlet stream, q_{LPO} , and the inlet stream, q_{in} , and is given in equation 3.1 [15].

$$FS = \frac{q_{LPO}}{q_{in}} \quad (3.1)$$

The difference in the outlet flow rates can affect the axial velocity inside the pipe, where the velocity in the outer part of the pipe may be faster or slower than the inner part of the pipe. It is therefore assumed that the axial velocity is divided into two regions, each having a constant velocity, see Figure 3.2, one for $r \leq R_i$ and one for $r > R_i$, and is given by equation 3.2. The assumption of two regions with constant velocities implies that there will be no friction between the fluid and the pipe as well as between the cylindrical and annular plug flows. The axial velocity is also assumed to be unaffected by the swirling behaviour of the flow and any turbulence is neglected by the use of time-averaged velocities [15].

$$v_z(r) = \begin{cases} \frac{q_{LPO}}{\pi R_i^2} & 0 \leq r \leq R_i \\ \frac{q_{HPO}}{\pi (R^2 - R_i^2)} & R_i < r \leq R \end{cases} \quad (3.2)$$

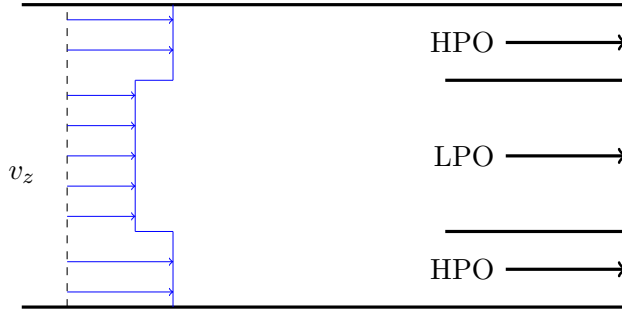


Figure 3.2: Velocity profile in the separator illustrating the velocity differences between the regions. Figure adapted from Tyvold [15].

Even though the axial velocity is a simplification of reality, it is expected to be sufficient for this case. The reason for this is that the aim is to estimate the separation performance and the axial velocity mainly affects the the degree of separation by determining the residence time of the droplets. The assumption of average axial velocity is therefore expected to be sufficient [15].

3.2.2 Tangential Velocity

The swirl-element generates a vortex inside the separator which forces the denser droplets towards the outer wall due to centrifugal forces. Since the centrifugal forces affects the droplets to a larger extent than the gravitational force, the gravitational acceleration, g , in equation 2.4 is substituted by the expression for centrifugal acceleration, as shown in equation 3.3.

$$a_c(r) = \frac{v_\theta(r)^2}{r} \quad (3.3)$$

where v_θ is the tangential velocity of the fluid. Experimental data obtained from experiments performed by Dirkwager [4] and van Campen [17] show that the tangential velocity can be described as a Rankine vortex. Such a vortex has a velocity profile that can be divided into two regions, one inner region with a solid rotation and one for the outer region with a free vortex [6]. In this model it is assumed that the velocity profile in the outer region will be simplified by keeping it constant. Figure 3.3 illustrates the region boundary at a radius R_c between the inner and outer boundary [15].

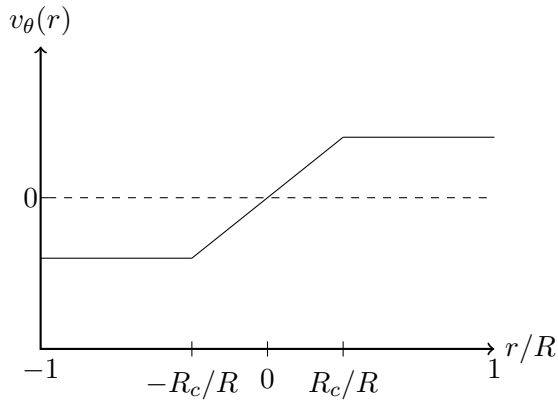


Figure 3.3: Profile of the tangential velocity, v_θ , for a Rankine vortex with inside a separator with radius R . Figure adapted from Tyvold [15].

From the assumptions above, the velocity in the tangential direction immediately downstream of the swirl element can thus be given by equation 3.4 [15]:

$$v_{\theta}^0(r) = \begin{cases} v_{\theta}^{max} \frac{r}{R_c} & , 0 \leq r \leq R_c \\ v_{\theta}^{max} & , R_c < r \leq R \end{cases} \quad (3.4)$$

Where v_{θ}^{max} is the maximum velocity and is assumed to be proportional to the velocity in the axial direction, v_z [15]:

$$v_{\theta}^{max} = \Omega v_z \quad (3.5)$$

Ω is the proportionality constant and is referred to as the *swirl number* in this project. The constant can either be calculated from the swirl element's geometry or determined experimentally. Due to the stress from the separator walls, the swirl, generated from the swirl element, is expected to lose momentum throughout the separator. By introducing a decay factor, C_{decay} , the loss of momentum is taken into account in the model and the tangential velocity can then be expressed as [4, 15]:

$$v_{\theta}(r, z) = v_{\theta}^0(r) \exp\left(\frac{-C_{decay} z}{2R}\right) \quad (3.6)$$

Smoothing the Tangential Velocity

In order to calculate the gas volume fraction (GVF) and the liquid volume fraction (LVF) in the LPO and the HPO, the critical inlet radius of an oil droplet, r_{in} , that is expected to travel to the edge of the radius, R_i , is found using the shooting method, see section 3.2.5. Since the radius for the gas-extraction pipe, R_i is larger than R_c , the oil droplet trajectory is expected to travel across the tangential velocity regions. The expression for the tangential velocity, given in equation 3.4, is discontinuous at R_c , which

can cause problems for the integrator function, described in section 3.2.5. This issue is solved by using the smoothing approximation by Balakrishna and Biegler [2, 15]:

$$\max(f(x), 0) = \frac{1}{2} \left[(f(x)^2 + \beta^2)^{1/2} + f(x) \right] \quad (3.7)$$

where β is the smoothing parameter. By rewriting equation 3.4 and applying the smoothing approximation, equation 3.7, the tangential velocity, v_θ^0 can be smoothed as shown in equation 3.8 [15].

$$v_\theta^0 = v_\theta^{max} - \max \left(v_\theta^{max} \left[1 - \frac{r}{R_c} \right], 0 \right) \quad (3.8)$$

In this project the transition radius between the regions is set to be $R_c = 0.25 R$ [15] and the smoothing parameter is set to 1. The smoothed function is likely to deviate from the original function around the transition area, but this deviation is assumed to be negligible and its effect on the separation performance is expected to be relatively small.

3.2.3 Radial Velocity

As mentioned in section 3.2.2, the centrifugal buoyancy force is expected to be the dominating force affecting the oil-droplets inside the separators. If the fluid is also assumed to be in the Stokes' regime and Stokes' law is valid, equation 2.4 can be rewritten to give the radial velocity of an oil-droplet, v_r :

$$v_r(r, z) = \frac{2r_d^2(\rho_d - \rho_c)}{9\mu} \frac{v_\theta^2(r, z)}{r} \quad (3.9)$$

Where r_d is the radius of the droplet, μ is the viscosity of the continuous phase, and ρ_c and ρ_d are the densities of the continuous phase and the dispersed droplets, respectively. The velocity presented from equation 3.9 is actually the relative velocity of the droplet relative to the continuous phase, but by neglecting the radial movement of the continuous, phase it is approximated as the absolute radial velocity [15]. The velocity only takes into account the centrifugal forces and neglects other mass transfer phenomena such as diffusion, because it is expected that inside a swirl separator the centrifugal forces will affect the droplets to a much larger extent compared to the other mass transfer laws [15].

3.2.4 Droplet size

From equation 3.9 it is clear that the droplet size affects the radial velocity thus affecting the degree of separation. van Campen [16] stated that the acceleration of a dispersed system can lead to droplet breakup and it is therefore necessary to have a relationship between the flow inside the separator and the droplet size. In this project the model presented by Matovu in his Master Thesis will be used for this relationship [8]. This model is based on van Campen's [16] discussions on droplet breakup for a liquid-liquid system even though a gas-liquid system is modeled in this project. The model for droplet breakup for a liquid-liquid system is, however, expected to yield satisfactory estimates. The relationship between the droplet size and the flow is expressed as [8]:

$$D_d = 0.725 \left(\frac{\sigma}{\rho_c} \right)^{3/5} \left(\frac{\pi^3 D_{sep}^7}{64 q_{in}^3} \right)^{2/5} \quad (3.10)$$

where σ is the interfacial tension on the droplets, ρ_c is the density of the

continuous phase, D_{sep} is the separator diameter and q_{in} is the separator inflow. In order to simplify the model, an inverse linear relationship between the droplet size and the inflow was used in equation 3.10, giving the following relationship [8]:

$$D_d = m q_{in} + c \quad (3.11)$$

The parameters m and c in equation 3.11 are slope and intercept, respectively. The parameters were determined by fitting them to experimental data [8].

3.2.5 Equation of Motion

As mentioned in section 3.2.2, in order to determine the separation efficiency the inlet position of an oil-droplet, r_{in} , that gives a separator exit radius of at least R_i has to be found and is done by integrating equation 3.9 from $t = 0$ to $t = \tau$. τ is the residence time of the droplet from the point it enters the separator at $z = 0$ until it exits the separator at $z = L$ with an axial velocity given in equation 3.2 and the radial velocity from equation 3.9 and is expressed as [15]:

$$\tau = \frac{\pi R_i L}{FS \cdot q_{in}} \quad (3.12)$$

L in equation 3.12 is the length of the separator between the swirl element and the start of the gas-extraction pipe.

The integration of the radial velocity is done in MATLAB with a fourth order explicit Runge-Kutta integrator with constant time steps. The integral time is divided into 10 equal time steps, $h = \tau/10$, and the radial

position of the droplet at r_{n+1} is calculated from the previous position, r_n [15]. The set up for the fourth Runge-Kutta integrator is given as [3]:

$$r_{n+1} = r_n + \frac{1}{6} (k_1 + 2k_2 + 2k_3 + k_4) \quad (3.13)$$

$$k_1 = v_r(t_n, r_n) h \quad (3.14)$$

$$k_2 = v_r\left(t_n + \frac{h}{2}, r_n + \frac{k_1}{2}\right) h \quad (3.15)$$

$$k_3 = v_r\left(t_n + \frac{h}{2}, r_n + \frac{k_2}{2}\right) h \quad (3.16)$$

$$k_4 = v_r(t_n + h, r_n + k_3) h \quad (3.17)$$

where $v_r(t, r)$ is the radial velocity of the droplet. The details of the Matlab function can be found in Appendix A.6.

The radial velocity is a function of the radial inlet position while the radial outlet position is fixed, which makes the differential equation a boundary value problem[15]. To solve this boundary value problem the *shooting method* is used in order to find the radial inlet position that yields an outlet position of at least $r = R_i$ by using the Newton-Raphson method [3]. The MATLAB function for the *shooting method* is given in Appendix A.7

When the inlet radial position, r_{in} , is found it is assumed that all oil-droplets entering above this position ($r > r_{in}$) will exit the separator through the heavy phase outlet, while all droplets entering below this position ($r < r_{in}$) will leave the separator through the light phase outlet. If it is also assumed that the oil-gas mixture has a uniform distribution of the dispersed phase in the r, θ -plane at the separator inlet and that droplet trajectories don't cross each other during the separation process,

the liquid volume fraction (LVF) of the HPO is expressed by [15]:

$$\alpha'_{o,HPO} = (1 - \alpha_{in}) \frac{(1 - FS) R_i^2 + FS (R_i^2 - r_{in}^2)}{(1 - FS) R_i^2} \quad (3.18)$$

The LFV in the LPO is derived from component mass balance and given as [15]:

$$\alpha'_{o,LPO} = \frac{1}{q_{LPO}} \left[(1 - \alpha_{in}) q_{in} - \alpha'_{o,HPO} q_{HPO} \right] \quad (3.19)$$

3.2.6 Re-Entrainment

In section 3.2 it was assumed that the axial flow could be divided into two regions, each with constant velocity, and that there is no net flux across the boundary between the regions. This is an oversimplification of the velocity compared to what is realistic. In reality it is expected that if, for example the pressure in the light phase outlet is lower than in the heavy phase outlet some fluid will be pulled across the boundary and exit through the LPO (and vice versa), see Figure 3.4. Tyvold compensated for this oversimplification by including a concept called re-entrainment [15].

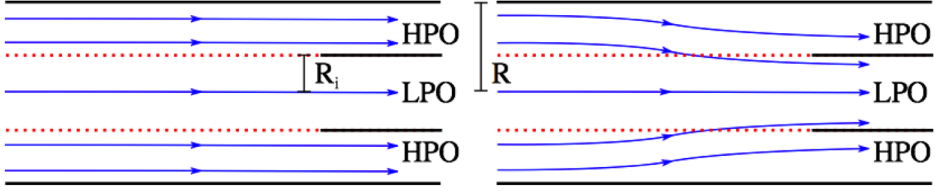


Figure 3.4: **Left:** Streamlines (blue) according to the model with no net flow across boundary, the pressure is lower at the LPO than in the HPO. **Right:** Streamlines with the re-entrainment concept included and a flow going inwards. Figure from Tyvold [15].

The concept of re-entrainment indicates that some oil that was initially separated from the gas will be re-entrained with the light-phase product and the opposite will be the case for low flow split between the outlet streams. The re-entrainment rate is assumed to depend on the difference in the axial velocities for LPO and HPO and that the re-entrainment will increase when the difference increases. The entrainment rate is given in equation 3.20 and through investigations on the different relationships between the re-entrainment rate and velocity differences, Tyvold found that a linear relationship gave the best agreement when compared to experimental data [15].

$$q_{re-en} = k_{re-en} \Delta v \quad (3.20)$$

Here Δv is the velocity difference between the inner (LPO) and the outer (HPO) region and k_{re-en} is a proportionality constant.

By using the re-entrainment concept equation 3.19 can be modified in order to compensate for the oversimplification of the model [15]:

$$\alpha_{o,LPO} = \frac{1}{q_{LPO}} \left[\alpha'_{o,LPO} (q_{in} - q_{re-en}) + \alpha'_{o,HPO} q_{re-en} \right] \quad (3.21)$$

From equation 3.21 it is possible to determine the gas volume fraction in the LPO and the HPO and are given as [15]:

$$\alpha_{LPO} = 1 - \alpha_{o,LPO} \quad (3.22)$$

$$\alpha_{HPO} = \frac{1}{q_{HPO}} [\alpha_{in} q_{in} - \alpha_{LPO} q_{LPO}] \quad (3.23)$$

3.2.7 Soave-Redlich-Kwong Equation of State

Gases are highly compressible fluids and their properties, such as density, changes a lot with varying pressures and temperatures. Since subsea systems often operate at conditions different than standard conditions ($T = 25^\circ\text{C}$ & $p = 1\text{atm}$) and it is therefore desirable to have a relationship between the gas properties and the state at which the gas is at. The Soave-Redlich-Kwong(SRK) equation of state [13], given in equation 3.24, is such an equation that can calculate the density of a gas given the temperature T and pressure p , and will be used in this model for the deliquidizer.

$$p = \frac{R_{gc}T}{V_m - b} - \frac{a \alpha}{V_m(V_m + b)} \quad (3.24)$$

where R_{gc} is the universal gas constant and V_m is the molar volume. The parameters α , a and b are defined as [13]:

$$a = \frac{0.42747 R_{gc}^2 T_c^2}{p_c} \quad (3.25)$$

$$b = \frac{0.08664 R_{gc} T_c}{p_c} \quad (3.26)$$

$$\alpha = \left(1 + (0.480 + 1.574\omega - 0.176\omega^2) \left(1 - T_r^{1/2} \right) \right) \quad (3.27)$$

$$T_r = \frac{T}{T_c} \quad (3.28)$$

where p_c is the critical pressure, T_c is the critical temperature, T_r is the reduced temperature and ω is the acentric factor.

Equation 3.24 can be rewritten as [13]:

$$Z^3 - Z^2 + Z(A - B - B^2) - AB = 0 \quad (3.29)$$

where Z is the compressibility factor and:

$$V_m = Z \frac{R_{gc} T}{p} \quad (3.30)$$

$$A = \frac{a p}{R_{gc}^2 T^2} \quad (3.31)$$

$$B = \frac{b p}{R_{gc} T} \quad (3.32)$$

Equation 3.29 can then be solved for Z and from equation 3.30 the molar volume can be found. The density of the gas, ρ , can then be calculated from:

$$\rho = \frac{M_m}{V_m} \quad (3.33)$$

where M_m is the molar mass of the gas. The full details of the MATLAB code used to solve the cubic SRK is given in Appendix A.5. The code is an adaption of Professor Sigurd Skogestad's code published on his web page [12]. The values for the acentric factor, critical temperature and pressure were found from *The Properties of GASES and LIQUIDS* [11].

3.2.8 Viscosity of mixtures

Equation 3.9 shows that the radial velocity of a droplet is inversely proportional to the viscosity of the mixture. The viscosity of a water-oil emulsion is dependent on the oil-water ratio and droplet size of the dispersed phase [1]. Tyvold therefore presented a model (see Figure 3.5 for illustration) that calculated the viscosity of the mixture as a function of the oil-cut in the separator for a given position in the separator [15] based on experimental data from van Campen [16].

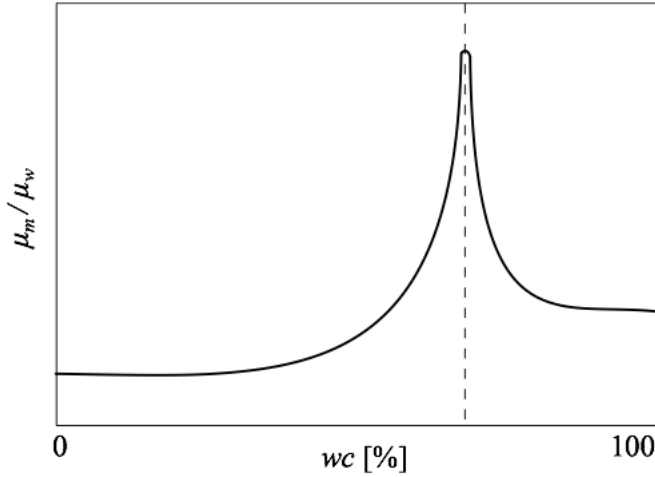


Figure 3.5: Illustration of the viscosity profile in an oil-water emulsion as a function of the water cut, wc , and the dashed line marks the phase inversion. Figure from Tyvold [15].

For a gas-liquid system it is extremely hard, close to impossible, to measure the viscosity of the mixture. To measure the viscosity of a mixture the components in the mixture have to be uniformly distributed, however with a gas this is close to impossible, because when measuring the viscosity in a rheometer, the rotating bob will force the gas upwards and out of the mixture. To overcome this problem, it is assumed in this project that the viscosity of the mixture is determined by the viscosity of the continuous phase, see Figure 3.6. This means that in a gas-in-oil mixture the viscosity will be given by the viscosity of the oil, μ_o , and in a oil-in-gas mixture, which will be the case in the deliquidizer, the viscosity is given by the viscosity of the gas, μ_g .

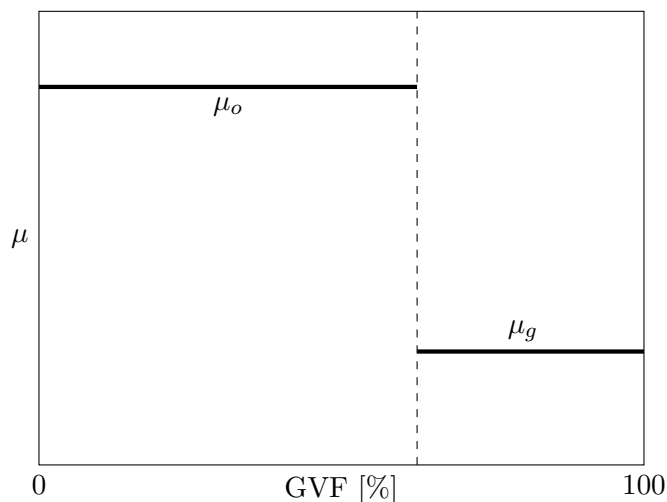


Figure 3.6: Illustration of the viscosity profile in this project as a function of the gas volume fraction, GVF, where μ_o is the viscosity of the oil and μ_g is the viscosity of the gas. The dashed line marks the phase inversion.

This assumption is expected to be reasonable due to the fact that there will be low fractions of the dispersed phase in the mixture which is not expected to have a large affect on the viscosity.

3.3 Model input

In the model generated above, there are a lot of parameters that need to be defined in order for the model to calculate the performance of the separator. Such inputs are the dimensions of the separator (section 3.3.1), empirical parameters (section 3.3.2) and the properties of the liquid-gas mixture (section 3.3.3).

The majority of the input is taken from Matovu [8] and Tyvold [15], the

rest of the parameters are, due to lack of data, adjusted in order to fit the model so that the numerical calculations converge.

3.3.1 Separator dimensions

The dimensions for the deliquidizer separator are given in Table 3.1. The length of the separator as well as the radius for the outer pipe are from Matovu [8] while the other two parameters are calculated and estimated.

Table 3.1: Separator dimensions.

Length	Outer pipe radius	Inner pipe radius	Swirl number
L [m]	R [m]	R_i [m]	Ω [-]
1.5	0.075	0.067	0.1

The radius of the inner pipe, R_i , was calculated in order to minimize re-entrainment at a flow split of 0.8. The axial flow rates in the LPO and HPO were therefore set to be equal when determining the radius.

The original swirl numbers presented by Tyvold [15] were a magnitude larger than the swirl number given in Table 3.1. The reason for the difference is convergency problems of the numerics with the original numbers, so the swirl number was reduced until the model converged. The small swirl number is reasonable due to the fact that in gas-liquid systems the density difference is so large that centrifugal force does not have to be at the same magnitude as liquid-liquid systems for sedimentation to occur.

3.3.2 Empirical Parameters

The empirical parameters are given in Table 3.2 and are from Matovu [8] and Tyvold [15].

Table 3.2: Empirical parameters for the deliquidizer.

Parameter	Value
C_{decay} [-]	0.04
k_{re-en} [m^2]	$2 \cdot 10^{-4}$
c [m]	0.0002
m [h/m^2]	$-0.6 \cdot 10^{-6}$

The decay factor, C_{decay} , was determined experimentally in Dirkzwager's Ph.D thesis[4]. The factor is dependent on the swirl number and is expected to decrease with increasing swirl numbers, meaning that the value is a rough approximation. The factor is also expected to depend on the viscosity of the system [15]. Even though the decay factor is estimated for a liquid-liquid system it is included in this model due to a lack of more realistic data for a gas-liquid system.

The re-entrainment proportionality constant, k_{re-en} , was determined by fitting the model to experimental data [15]. This is also based on a liquid-liquid system and is expected to be somewhat different in a gas-liquid system. However, due to lack of data for a gas-liquid system this value will also be included in the model.

The slope, m and the intercept, c , from equation 3.11 was calculated by fitting the model to experimental data by Matovu [8].

3.3.3 Fluid Properties

The properties of the fluid are one of the most important properties in order for the model to determine the separation performance. In this gas-liquid system the gas used is Methane and the liquid is crude oil made up of *refined mineral oil blended with zinc free additives* [15]. The properties are presented in Table 3.3 where the properties for the oil is taken from Tyvold [15] and the viscosity for methane is taken from the safety data sheet from the gas provider *Matheson* [7].

Table 3.3: Properties of the oil and methane gas used in the model.

Fluid	Density [kg/m^3]	Viscosity [$mPa \cdot s$]
Oil	881	8.8
Methane	-	0.0118

The density for Methane is not given in Table 3.3 and the reason for this is that the density is calculated using the SRK equation of state, see equation 3.24 section 3.2.7. The density is through this equation dependent on the operational conditions, which will be temperature and pressure. In this project the temperature and pressure are specified to be $T = 50^\circ\text{C}$ and $p = 50$ bar respectively.

4 Results & Discussion

In this chapter the results from the simulations are presented and interpreted. The model was first compared against experimental data from industry in order to get an indication that the model gives reasonable results, section 4.1. The effect of flow rate and flow split on the separation performance are analysed and interpreted in sections 4.2 and 4.3, respectively.

All the simulations are done in MATLAB and the scripts used are given in Appendix A.

4.1 Model vs Experimental data

The focus of this section is to compare the results from the model simulations with the experimental data in order to help tune the model and get an indication that the models shows results that are comparable to actual separators. The experimental data from the industry are given in Figures B.1, B.2 and B.3 in Appendix B. Since the data provided are transient while the model is steady-state, time samples had to be chosen and the respective parameters had to be calculated in order to conduct any comparison with the model. The parameters inlet flow, q_{in} , flow split, FS , inlet gas fraction, α_{in} , gas volume fraction in the light phase outlet, GVF_{LPO} , and the liquid volume fraction in the heavy phase outlet, LVF_{HPO} , were calculated for three time samples. The parameters that were calculated from the experimental and are given in Table 4.1 were chosen at the times 1296 hours ($q_{in} = 204.9$), 838 hours ($q_{in} = 208.1$) and 1000 hours ($q_{in} = 217.8$), from Figure B.1 in Appendix B.

The calculated values for flow split, inlet flow rate and inlet gas fraction from the experimental data were used as inputs to the model in order to calculate the gas volume fraction in the light phase outlet and the liquid volume fraction in the heavy phase outlet. The calculated experimental data and the results from the model are given in Table 4.1.

Table 4.1: Comparison between experimental data and model results. Flow split = 0.97 and inlet gas fraction $\alpha_{in} = 0.83$.

Inlet flow $q_{in} [m^3/h]$	$GV_{FLPO} [-]$	$GV_{FLPO} [-]$	Difference [%]	$LV_{FHPO} [-]$	$LV_{FHPO} [-]$	Difference [%]
	Exp.data	Model Results		Exp.data	Model Results	
204.9	0.85	0.86	1.16	0.71	1.00	33.92
208.1	0.85	0.86	1.16	0.83	1.00	18.58
217.8	0.85	0.86	1.16	0.77	1.00	26.99

From Table 4.1 it is clear that the model operates with a good precision for the gas volume fraction in the light phase outlet, only having a difference from the experimental data of about 1%. The model does, however, have less satisfactory prediction of the liquid volume fraction in the heavy phase, having between 18 % - 34% difference from the experimental data.

A reason for the large difference in liquid volume fraction in the HPO between the experimental data and the simulated data from the model can be a result of different separator dimensions. The dimensions of the deliquidizer in this project are taken from Matovu's work [8] and are expected to differ from the dimensions of the separator used to obtain the experimental data. The separation performance depends on the dimensions of the separations where different length will give different residence times, which will affect the performance. A difference in the radius of the gas-extraction pipe will also change the separation performance, since a larger radius will increase the distance a droplet has to travel in order

to get separated, while a smaller radius will decrease the distance for the droplet and affecting the overall performance. The separator used for the experimental data also includes a degassing boot, that acts as a liquid hold-up and is level controlled. Since the boot is level controlled, this will effect the flow rate out through the heavy phase outlet and is assumed to affect the liquid volume fraction in the HPO, resulting in difference between the results from the model and the experimental data.

The parameters used in the deliquidizer models are also believed to be a reason behind the deviation between the simulated results of the model and the experimental data. These parameters are from the work of Tyvold [15] and Matovu [8] and are based on liquid-liquid systems and even though they are included and assumed to give reasonable estimates, they will introduce error to the model. The parameters describing the droplet size are expected to have one of the largest effect on the error. The function for the droplet size is a linear relationship with the inlet flow rate and because of this the droplet size will at some point become zero or even negative, which is highly unrealistic. The size of the droplets is expected to go asymptotically towards zero instead of having a linear relationship, which will give an error in the droplet size estimation that will propagate to the separation performance. The value for the swirl number used to generate the vortex inside the separator has been chosen so that the numerics in the model will converge and will therefore be different from the experimental data. This will introduce an error in the model and causing the deviations seen in Table 4.1.

4.2 Flow rate effect

The performance of the deliquidizer was tested for the effect of the inlet flow rate, and the results are given in Figure 4.1. The inlet gas fraction is $\alpha_{in} = 0.8$ and the flow split was put to $FS = 0.8$.

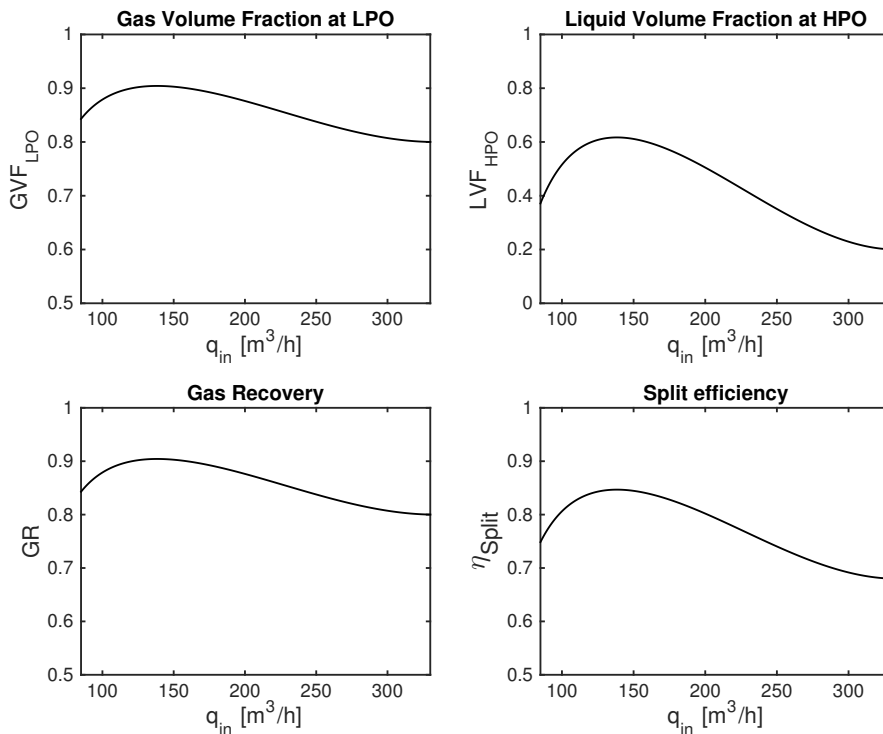


Figure 4.1: Deliquidizer performance with inlet gas fraction of 0.8 and flow split of 0.8 as a function of inlet flow rate, q_{in} .

From the figure presented above, the profile of the gas volume fraction in the LPO shows an expected trend with increasing flow rate. The GVF initially starts to increase with increasing flow rate to a maximum value of

GVF at a given flow rate, followed by a decrease in GVF when continuing the increase in flow rate. Low flow rates generates low tangential velocities, which is a major driving force for the separation, thus giving low initial separation and low GVF. As the inlet flow rate increases the tangential velocity will increase, generating a larger force pulling the oil-droplets towards the separator wall. The result of an increasing flow rate will thus be a greater separation performance. This will be the case until a maximum GVF is reached for a given flow rate and for the deliquidizer it happens at $q_{in} = 140 \text{ m}^3/h$ giving $GVF = 0.90$. At this flow rate an equilibrium of underlying forces will happen.

The residence time and droplet size both depend on the inlet flow rate and will both decrease with increasing flow rate, see Figures C.1 and C.2 in Appendix C. With a decreasing droplet size, the mass in which the centrifugal acceleration will affect will decrease resulting in a lower radial velocity for the droplet. Reduced residence time results in a shorter time that the droplet has to travel from r_{in} to R_i in order to be separated, which means that a droplet must have a higher r_{in} if separation of the droplet is to happen. Increasing the flow rate even more will therefore result in reduced separation efficiency because at these flow rates the combined effect of droplet size and residence time will be greater than the tangential velocity.

The decrease of GVF starts to flatten out at flow rates above $250 \text{ m}^3/h$. The reason for this may be that the decrease in residence time also start to flatten out with high flow rates (Figure C.1 in Appendix C). This may then result in an equal effect from the continued increase of the tangential velocity and the decrease in the droplet size that will result in the GVF decrease flattening out.

The profiles of the other subplots in Figure 4.1 come as a result of the profile of the GVF. The recovery of gas increases as the gas volume fraction in the LPO increases and is because a larger amount of gas exits through the desired outlet. The gas recovery will decrease with low GVF since a lot more oil has not been separated, thus making the gas leave through the HPO. The liquid volume fraction in the HPO will increase as a result of an increasing GVF because the separation performance is increased, making more oil leave the separator through the HPO. On the other hand the LVF will decrease with decreasing GVF since less liquid will then be separated from the gas phase. When the GVF and LVF increases the split efficiency will also increase, because the amount of liquid that exits the separator through its desired outlet increases.

4.3 Flow split effect

The purity in the product streams can be affected by manipulating the flow splits, resulting in a trade off between the purity in the LPO and the HPO. The performance of the separator was therefore tested for the effect of the flow split and the results are given in Figure 4.2. The inlet gas fraction is 0.8 and the inlet flow rate is $140 \text{ m}^3/h$.

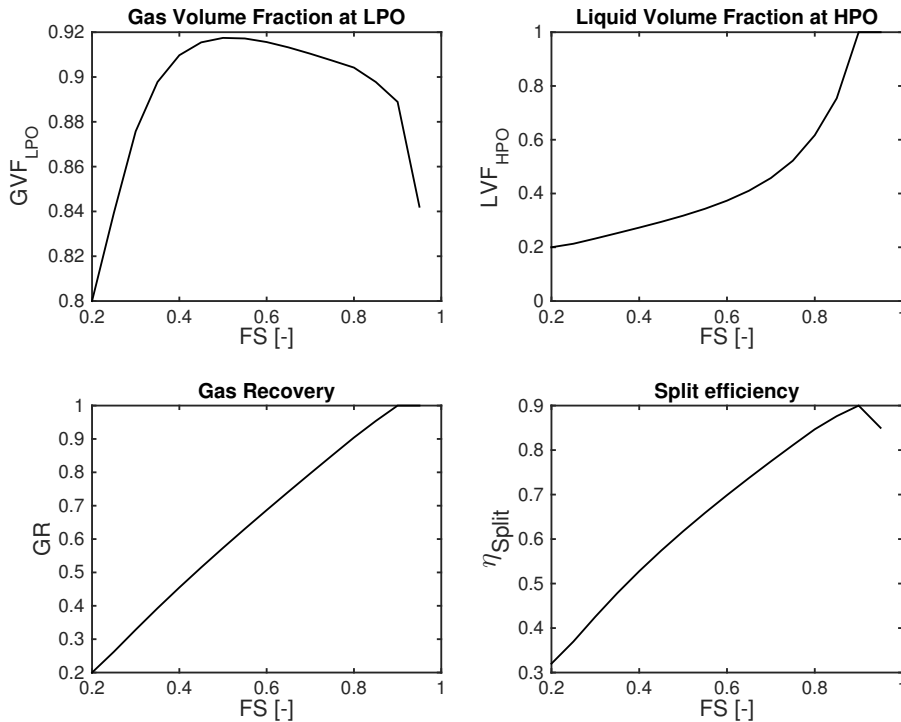


Figure 4.2: Deliquidizer performance with inlet gas fraction of 0.8 and flow rate of 140 m³/h as a function of flow split, FS .

The profile for the gas volume fraction in the light phase outlet shows an unexpected result at low flow splits. It is expected that at low flow splits the impurity is shifted towards the heavy phase outlet giving pure LPO streams, which is not the case in the figure. This leads to a suspicion that the model is operating outside its operating area and fails at low flow splits. A lot of the parameters in the model are based on a liquid-liquid system, and they may therefore be very sensitive toward changes in flow split, oil fraction and flow rate. Since the expected area of operation for

a deliquidizer is at higher flow splits (above $FS = 0.5$) it will not be in the scope of this project to investigate the reasons for the error. The investigations will be conducted in the future.

From a flow split of 0.5 and above, the figure of gas volume fraction in the light phase outlet is as expected. When increasing the flow split, the volumetric flow rate out through the LPO will increase while the volumetric flow rate out through the heavy phase outlet will decrease. This will direct the impurities away from the HPO and towards the LPO giving an increase of liquid volume fraction in the HPO and a decrease of GVF in the LPO.

The gas recovery will increase with increasing flow split which is as expected, since when increasing the flow split more will flow out through the LPO meaning that more gas will flow out through its desired outlet. The split efficiency also increases with increasing flow split. This is logical because when the flow split increases the flow out through the HPO will decrease, directing impurities away from the HPO, resulting in more oil leaving its desired outlet. The split efficiency does however start to decrease at about $FS = 0.9$. This is because the LVF in the HPO is 1 at this point, meaning that only oil is in the HPO and by increasing the flow split, some oil will be directed away from its desired outlet and into the LPO.

5 Conclusion

In this project a deliquidizer that separates oil from a gas-rich stream has been studied. The models developed for the separator are based on average velocities for the oil droplets, centrifugal forces and drag forces that are approximated by Stokes' law. The droplet size in the deliquidizer is assumed to have a linear relationship with the inlet flow rate.

The model for the separator was compared towards experimental data obtained from industry. The model showed a satisfying accuracy in estimating the gas volume fraction in the light phase outlet with a deviation of about 1%. For the liquid volume fraction in the heavy phase outlet the model did however seem to overestimate the separation, giving a deviation of 18% - 34% from the experimental data.

The effect of varying flow rates and flow splits on the separation performance was also tested and analysed. The performance as a function of varying flow rates was as expected; with an increase in separation efficiency with increasing flow until a maximum was reached, followed by a decrease in efficiency with further flow increase. The performance of the separator as a function of varying flow split showed unexpected results at low flow splits and satisfactory results with higher flow splits ($FS > 0.5$). The operating area of the deliquidizer is expected to be above 0.5 and the issues with low flow splits were neglected in this project, but an investigation in the reason behind this error is recommended for further work.

Even though the model was compared towards experimental data, the obtained data was not sufficient enough to validate the model. The experimental data was only used in tuning the model and to give an indication that the model is on right-track giving reasonable results. A more com-

prehensive data set is therefore needed in order to validate the model.

5.1 Further Work

The various model parameters are highly sensitive to changes in model input and are chosen in order to make the model numerics converge and therefore they have minimal support from experimental data. This introduces an error in the model simulations and in order to improve the model and reduce any errors, experimental data should be found and used to support these parameters. The lack of experimental data for oil-gas systems can however lead to difficulties in order to obtain values for the necessary parameters.

The droplet size has, as mentioned above, a linear relationship with respect to the inlet flow. This means that the droplet size can eventually become zero or have a negative size at certain values of the inlet flow rate, which is highly unrealistic. It is more realistic that the droplet size will go asymptotically towards zero and investigations to improve the droplet size function in order to give it such a property is therefore recommended and expected to help improve the model.

An investigation of the model of at low flow splits should also be conducted in order to obtain a model working over the entire range of the flow splits.

Optimization of the separator should also be conducted in order to find the optimized operating conditions for the separator for a given set of operational constraints, followed by proposing a control structure.

Bibliography

- [1] ARIRACHAKARAN, S., OGLESBY, K. D., MALINOWSKY, M. S., SHOHAM, O., AND BRILL, J. P. An Analysis of Oil/Water Flow Phenomena in Horizontal Pipes. *SPE Production Operations Symposium 18836* (1989), 155. URL: <https://www.onepetro.org/conference-paper/SPE-18836-MS>.
- [2] BALAKRISHNA, S., AND BIEGLER, L. T. Targeting strategies for the synthesis and energy integration of nonisothermal reactor networks. *Industrial & Engineering Chemistry Research* 38, 3 (1992), 2152–2164. URL: <http://pubs.acs.org/doi/abs/10.1021/ie00009a013>.
- [3] CONSTANTINIDES, A., AND MOSTOUFI, N. *Numerical Methods for Chemical Engineers with MATLAB Applications*, 1 ed. Prentice Hall PTR, Upper Saddle River, N.J, 1999.
- [4] DIRKZWAGER, M. *A New Axial Cyclone Design for Fluid-Fluid Separation*. Ph.d, Delft University of Technology, 1996.
- [5] FMC-TECHNOLOGIES. Separation Systems- Subsea Separation. URL: <http://www.fmctechnologies.com/en/SeparationSystems/Solutions/SubseaSeparation.aspx>, Entered: 13.12.2015.
- [6] GIAIOTTI, D. B., AND STEL, F. The Rankine Vortex Model. *October* (2006), 1–14. URL: http://www.fisica.uniud.it/~osmer/RnD{_}group/Giaiotti/PhD{_}EFM/103{_}rankine.pdf.
- [7] MATHESON. Methane Safety Data Sheet, 2015. URL: <http://www.chemadvisor.com/Matheson/database/msds/00244226000800003.PDF>, Entered: 08.12.2015.

- [8] MATOVU, F. *Modelling and Optimization of Compact Sub-sea Separators*. Master thesis, Norwegian University of Science and Technology, Trondheim, 2015.
- [9] MØRK, P. *Overflate og kolloidkjemi: grunnleggende prinsipper og teorier*, 4th ed. Department of Chemical Engineering, Norwegian University of Science and Technology, 2004.
- [10] ØXNEVAD, D. Statoil's Subsea Technology Challenges: A history of global leadership in Subsea Processing.
- [11] POLING, B. E., PRAUSNITZ, J. M., AND O'CONNELL, J. P. *The Properties of GASES AND LIQUIDS*, 5th ed. McGraw-Hill, New York, 2007.
- [12] SKOGESTAD, S. Sigurd Skogestad's Homepage. URL: <http://www.nt.ntnu.no/users/skoge/book-cep/matlab/srk-flash/>, Entered: 01.10.2015.
- [13] SOAVE, G. Equilibrium constants from a modified Redlich-Kwong equation of state. *Chemical Engineering Science* 27, 6 (1972), 1197 – 1203.
- [14] STATOIL. Subsea Processing on Tordis. URL: <http://www.statoil.com/en/TechnologyInnovation/FieldDevelopment/AboutSubsea/SubseaProcessingOnTordisIOR/Pages/default.aspx>, Entered: 13.12.2015.
- [15] TYVOLD, P. *Modeling and Optimization of a Subsea Oil-Water Separation System*. Master thesis, Norwegian University of Science and Technology, Trondheim, 2015.

- [16] VAN CAMPEN, L. *Bulk Dynamics of Droplets in Liquid-Liquid Axial Cyclones*. Ph.d, Delft University of Technology, 2014. URL: <http://repository.tudelft.nl/view/ir/uuid{\%3Abf295221-4e6e-4663-b046-79da13325243/>.
- [17] VAN CAMPEN, L., MUDDE, R. F., SLOT, J., AND HOEIJMAKERS, H. A Numerical and Experimental Survey of a Liquid-Liquid Axial Cyclone. *International Journal of Chemical Reactor Engineering* 10, 1 (2012). URL: <http://www.degruyter.com/view/j/ijcre.2012.10.issue-1/1542-6580.3003/1542-6580.3003.xml>.

A MATLAB-scripts

The MATLAB-scripts used in the simulation of the deliquidizer are presented in this appendix. All the scripts are adaptations of the models used by Tyvold [15], except the script for the Soave-Redlich Kwong, Appendix A.5, which is adapted from the script made by Skogestad [12].

A.1 Main Function

The script *Swirl_driver_deliq.m* calls the functions given in the sections below in order to plot the results and analyse the performance.

```
%      This script calls and runs the function swirl_func3_deliq
%      which will do all calculations for the separation
%      process in the Deliquidizer. This script will then
%      generate the results and graphs from the process.

%      Author: Torstein Bishop, Department of Chemical
%      Engineering, NTNU. Fall 2015.

clc
clear all
%% Performing the calculations of the separator
Vg_in = 0.8; %Gas fraction into separator
qin = [85:1:330]; %Inlet flow-rate into separator [m3/h]
FS = [0.2:0.05:0.95]; %Flow split between top and bottom outlet stream.

Vg_HPO=zeros(length(qin),length(FS)); % HPO gas cut
Vg_LPO=zeros(length(qin),length(FS)); % LPO gas cut
GR=zeros(length(qin),length(FS)); % Gas Recovery
```

```

Esplit=zeros(length(qin),length(FS));    % Split efficiency

for i = 1:length(qin)
    for j = 1:length(FS)

        [Vg_LPO(i,j),Vg_HPO(i,j),GR(i,j),Esplit(i,j),qen(i,j)]...
            = swirl_func3_deliq(Vg_in,qin(i)/3600,FS(j));

    end
end

%% Generating plots
% GVF, LVF, GR and Esplit as a function of qin, FS = 0.8 (index = 13)
figure(1)
subplot(2,2,1)
plot(qin,Vg_LPO(:,13),'k')
axis([85 330 0.5 1])
xlabel('q- $\{in\}$  [ $m^3/h$ '],'FontSize',12)
ylabel('GVF- $\{LPO\}$ ','FontSize',12)
title('Gas Volume Fraction at LPO')

subplot(2,2,2)
plot(qin,1-Vg_HPO(:,13),'k')
axis([85 330 0 1])
xlabel('q- $\{in\}$  [ $m^3/h$ '],'FontSize',12)
ylabel('LVF- $\{HPO\}$ ','FontSize',12)
title('Liquid Volume Fraction at HPO')

subplot(2,2,3)
plot(qin,GR(:,13),'k')
xlabel('q- $\{in\}$  [ $m^3/h$ '],'FontSize',12)
ylabel('GR','FontSize',12)
title('Gas Recovery')
axis([85 330 0.5 1])

```

```
subplot(2,2,4)
plot(qin,Esplit(:,13),'k')
xlabel('q_{in} [m^3/h]', 'FontSize',12)
ylabel('\eta_{Split}', 'FontSize',15)
title('Split efficiency')
axis([85 330 0.5 1])

% GVF,LVF, GR and Esplit as a function of FS, qin = 140 (index = 56)
figure(2)
subplot(2,2,1)
plot(FS,Vg_LPO(56,:), 'k')
xlabel('FS [-]', 'FontSize',12)
ylabel('GVF_{LPO}', 'FontSize',12)
title('Gas Volume Fraction at LPO')

subplot(2,2,2)
plot(FS,1-Vg_HPO(56,:), 'k')
%axis([85 350 0 1])
xlabel('FS [-]', 'FontSize',12)
ylabel('LVF_{HPO}', 'FontSize',12)
title('Liquid Volume Fraction at HPO')

subplot(2,2,3)
plot(FS,GR(56,:), 'k')
xlabel('FS [-]', 'FontSize',12)
ylabel('GR', 'FontSize',12)
title('Gas Recovery')
%axis([85 350 0.5 1])

subplot(2,2,4)
plot(FS,Esplit(56,:), 'k')
xlabel('FS [-]', 'FontSize',12)
ylabel('\eta_{Split}', 'FontSize',15)
title('Split efficiency')
%axis([85 350 0.5 1])
```

```

%% Analysis and Separator profiles
Lsw = 1.5; %Separator length
Ro = 0.075; % Separator radius
Ri = sqrt(4/5)*Ro; % Gas-extraction radius

rad = [0.001:0.001:0.075]; % Vector of radius of separator
l = [0:0.1:1.5]; % Vector of length through separator
FS2 = 0.8; %Flow split
for i = 1:length(qin)

    % Tangential velocity equations
    Rc=0.25*Ro; %Critical radius
    va=(qin(i)/3600)/(pi*Ro^2); %Axial velocity

    k=0.1; %swirl number
    vt0(i)=k*va; % Tangential velocity immediately after the swirl element
    vt_quad(i) = (vt0(i))^2;

    qi=FS2*(qin(i)/3600); %Light phase out flow
    qo=(qin(i)/3600)-qi; %Heavy phase out flow

    ta(i)=(pi*Ri^2*Lsw)/qi; %Residence time

%
    for j = 1:length(rad)
        for k = 1:length(l)
            % Finding the tangential velocity at a given place in the
            % separator
            f2=(vt0(i)*exp(-0.04*l(k)/(2*Ro)))^2/rad(j);
            f1=(vt0(i)*exp(-0.04*l(k)/(2*Ro))/Rc)^2*rad(j);
            f=f2-f1;

```

```

        beta=1; %Smoothing parameter
        ac(i,j,k)=f2-0.5*((f^2+beta^2)^.5+f);
    end
end

% Droplet radius equations
rd(i) = (-0.6*(qin(i))*1E-6+0.0002)/2;

% Re-entrainment equations

u_LPO(i)=qi/(pi*Ri^2);
u_HPO(i)=qo/(pi*(Ro^2-Ri^2));
du=u_LPO(i)-u_HPO(i);
kreen=2*10^-4; %Re-entrainment proportionality constant
qen1(i)=kreen*du;

end

figure(5)
plot(qin,vt0,qin,vt_quad)
xlabel('q_{in}')
ylabel('Tangential velocity after swirl-element and quadratic')

rd1 = rd*1E6;

figure(6)
plot(qin,rd1,'k')
xlabel('q_{in} [m^3/h]', 'FontSize',12)
ylabel('Droplet radius [\mum]', 'FontSize',12)
axis([85 330 0 80])

figure(7)
plot(qin,qen1)
xlabel('q_{in}')
ylabel('Re-entrainment rate')

```

```
figure(8)
plot(qin,u_LPO,qin, u_HPO,qin,vt0)
xlabel('q_{in}')
ylabel('Axial velocity')
legend('LPO velocity', 'HPO velocity', 'v_{\theta}^{\max}')

% Centripetal acceleration at qin=85
ac85 = squeeze(ac(1, :, :));

figure(9)
%surf(1,rad,ac85)
surf(1,rad,ac85)
ylabel('Separator radius [m]')
xlabel('Separator length [m]')
zlabel('a_{c} [m/s^{2}]')
title('q_{in} = 85 m^{3}/h')

% Centripetal acceleration at qin=140
ac140 = squeeze(ac(56, :, :));

%
figure(10)
surf(1,rad,ac140)
ylabel('Separator radius [m]')
xlabel('Separator length [m]')
zlabel('a_{c} [m/s^{2}]')
title('q_{in} = 140 m^{3}/h')
%
% % Centripetal acceleration at qin=217
ac217 = squeeze(ac(133, :, :));

figure(11)
```

```

surf(1,rad,ac217)
ylabel('Separator radius [m]')
xlabel('Separator length [m]')
zlabel('a-{c} [m/s^{2}]')
title('q-{in} = 217 m^{3}/h')
%
%
% %Centripetal acceleration at q = 300
ac300 = squeeze(ac(216, :, :));

figure(12)
surf(1,rad,ac300)
ylabel('Separator radius [m]')
xlabel('Separator length [m]')
zlabel('a-{c} [m/s^{2}]')
title('q-{in} = 300 m^{3}/h')

figure(13)
plot(qin,ta,'k')
xlabel('q-{in} [m^3/h]', 'FontSize',12)
ylabel('Residence time, \tau, [s]', 'FontSize',12)
axis([85 330 0.2 1.2])

```

A.2 Separator Performance Function

The function *swirl_func3_deliq.m* calculates the gas recovery and split efficiency given a set of inlet conditions. It also initiates the shooting-method in order to find the maximum radius a droplet can have in order to separate.

```

function [Vg_LPO,Vg_HPO,GR,Esplit,qen]=...
    swirl_func3_deliq(Vg_in,qin,FS)

```

```

Lsw=1.5; %Separator length
Ro=0.075; %Separator radius
Ri= sqrt(4/5)*Ro; %Radius for gas-extraction pipe

qi=FS*qin; %Light phase out flow
qo=qin-qi; %Heavy phase out flow
ta=(pi*Ri^2*Lsw)/qi; % Residence time

%%
%Finding rin=r(t0) that gives r(ta)=Ri
h=ta/10;%Amount of steps
rin_0= 0.00001;% Initial guess
in=[qin,Ro,Ri,Vg_in,ta,rin_0,FS];
rho=1; %Under-relaxation parameter
tol=10^-10*Ri; %Tolerance allowed in interation
[T,X]=shooting_deliq(@swirl_sep2_deliq,[0,ta],h,Ri,rin_0,rho,tol,in);

rin=X(1,1); %Inlet radius for droplet

[Vg_LPO,Vg_HPO,qen]=DeLiquidizer(qin,Vg_in,FS,rin,[Lsw;Ro;Ri]);
Vo_LPO=1-Vg_LPO; Vo_HPO=1-Vg_HPO;

GR=Vg_LPO*qi/((Vg_in)*qin); % Gas Recovery
Esplit=1-((1-Vg_LPO)*qi+Vg_HPO*qo)/qin; % Split efficiency

```

A.3 The Governing Equations

The function *swirl_sep2_deliq* contains the majority of the governing equations for the deliquidizer. The function calculates the radial velocity of a droplet and initiates the function containing the Soave-Redlich-Kwong

equation of state in order to calculate the gas density.

```
function [vr]=swirl_sep2_deliq(t,x,in)
qin=in(1);
Ro=in(2);
Ri=in(3);
Vg_in=in(4);
ta=in(5);
rin=in(6);
FS=in(7);

% Filling in component data needed to calculate the density of the gas
% found from The properties of Gases and Liquids fifth edition.
compData.Pc = 45.99e5; % [Pa], Critical Pressure
compData.Tc = 190.56; % [K], Critical Temperature
compData.w = 0.011; % Acentric factor
compData.Cp = 0; % Not used in any calculations yet
compData.Tref = 273.15; % [K]
compData.Mm = 16.043; % [g/mol]

P = 50e5; % [Pa] Pressure in separation system
T = 50+273; % [K] Assumed temperature in separation system
y = 1; % Assume only methane in gas phase

% Calling SRK-EOS for density calculations
[Z, RHO] = SRK(y, T, P, 'vapor', compData);

rhog=RHO; %kg/m^3, density for gas
rhoo=881; %kg/m^3, density for oil

r=x(1);

Rc=0.25*Ro; %Critical radius
```

```

va=qin/(pi*Ro^2); % Initial axial velocity

k=0.1; % Swirl number

vt0=k*va; %Initial tangential velocity

rd = (-0.6*(qin*3600)*1E-6+0.0002)/2; % Droplet size

Visc_gas = 0.00001118; % Gas viscosity

mum=Visc_gas;

%Smooth centrifugal acceleration
f2=(vt0*exp(-0.04*va*t/(2*Ro)))^2/r;
f1=(vt0*exp(-0.04*va*t/(2*Ro))/Rc)^2*r;
f=f2-f1;
beta=1; %Smoothing parameter
ac=f2-0.5*((f^2+beta^2)^.5+f); %Centrifugal acceleration

%Radial velocity of droplet
vr=(2/9*(rhoo-rhog)*rd^2/mum)*ac; %Original model

end

```

A.4 Composition Calculations

The function *DeLiquidizer* calculates the outlet conditions in terms of composition in the outlet streams given a set of inlet conditions. The compositions are calculated from the smallest radial inlet position a droplet can in order to exit through the HPO.

```

function [Vg_LPO,Vg_HPO,qen]=DeLiquidizer(qin,Vg_in,FS,rin,p3)

Ro=p3(2);Ri=p3(3);

qi=FS*qin;           %Light phase out flow
qo=qin-qi;           %Heavy phase out flow

% Volume fraction of oil in outlets before
% the re-entrainment is accounted for
Vo_HPO=(1-Vg_in)*(((1-FS)*Ri^2+FS*(Ri^2-rin^2))/((1-FS)*Ri^2));
Vo_LPO=((1-Vg_in)*qin-Vo_HPO*qo)/qi;

% Velocities needed for re-entrainment
u_LPO=qi/(pi*Ri^2);
u_HPO=qo/(pi*(Ro^2-Ri^2));
du=u_LPO-u_HPO;
k=2*10^-4; % Re-entrainment proportionality coefficient
qen=k*du;

%Adding re-entrainment to fraction equations
if du>=0
    Vo_LPO=(Vo_LPO*(qi-qen)+Vo_HPO*qen)/qi;
    Vo_HPO=((1-Vg_in)*qin-Vo_LPO*qi)/qo;
else
    Vo_HPO=(Vo_HPO*(qi+qen)-Vo_LPO*qen)/qi;
end

% Restrict oil volume fraction in HPO
% to range Vw_in->1
if Vo_HPO>1
    Vo_HPO=1;
elseif Vo_HPO<(1-Vg_in)
    Vo_HPO=(1-Vg_in);
end

```

```

Vo_LPO=((1-Vg_in)*qin-Vo_HPO*qo)/qi;%Oil composition in LPO

Vg_LPO=1-Vo_LPO; %Gas composition in LPO
Vg_HPO=1-Vo_HPO; %Gas composition in HPO
end

```

A.5 Soave-Redlich-Kwong Equation of State

The function *SRK* calculates the density of the gas given the temperature, pressure and gas composition of the system, as well as important component parameters.

```

function [ Z, RHO, V ] = SRK(x,T,P,Phase,compData )
% This is a remake of Andreas Linhart and Sigurd Skogestads
% implementation of the SRK-EOS and is adapted for specialization project
% fall 2015.

%Author: Torstein Bishop, Department of Chemical Engineering, NTNU. Fall
%2015.

% IN: molefraction of mixture (x), Pressure (P) [Pa], Temperature [K],
% phase of mixture and various component data (Tc,Pc, CP, w).

%OUT: Compressibility, Z, and density, rho, [kg/m3].

% Checking for number of components and gathering compData
NC = length(x);

%Checking for consistent mole fractions
if NC == 1 && sum(x) <1
    disp('Inconsistent mole fractions')
end

```

```
%Here: SRK binary interaction parameters set to zero
kinteraction=zeros(NC,NC);

% initialize
% liquid=1;vapor=2; Not sure if this part is needed
R = 8.314; % [J/K*mol]

Pc=compData.Pc; %Critical Pressure
Tc=compData.Tc; %Critical Temperature
w=compData.w; % Acentric factor
ZRA=0.29056-0.08775*w; % Rackett compressibility factor.
Cp=compData.Cp;
Tref=compData.Tref; % Reference temperature
Mm=compData.Mm/1000; % Molar mass for the components

% Calculating important parameters needed to solve system
Tre=T./Tc;
Pre=P./Pc;
m=0.480+1.574.*w-0.176.*w.^2;
a=(1+m.*(1-Tre.^0.5)).^2;
Ap=0.42747.*a.*Pre./Tre.^2;
Bp=0.08664.*Pre./Tre;

% Start calculations
% Binary a's:
Ab=zeros(NC,NC);
for i=1:NC
    for j=1:NC
        Ab(i,j)=(Ap(i)*Ap(j))^0.5;
    end
end
% Mixture a and b
A=0;
```

```

for i=1:NC
    for j=1:NC
        A=A+x(i)*x(j)*Ab(i,j)*(1-kinteraction(i,j));
    end
end
B=0;
for i=1:NC
    B=B+x(i)*Bp(i);
end

% Solve cubic equation to find compressibility Z = P*V/(R*T)
Zall=roots([1 -1 A-B-B^2 -A*B]);
% use real roots only
    Zreal=[];
    for i=1:3
        if isreal(Zall(i))==1
            Zreal=[Zreal Zall(i)];
        end
    end

    %disp(Zreal)
% Select right root depending on phase
if strcmp(Phase,'liquid')
    Z=min(Zreal);
elseif strcmp(Phase,'vapor')
    Z=max(Zreal);
else
    disp('error in specifying phase')
end

% Density (more precisely: molar volume)
MM = 0;
if strcmp(Phase,'liquid')%Correct liquid SRK-volume using Peneleoux...
    %correction

```

```

c=0;
for i=1:NC
c=c+x(i) * (0.40768 * (0.29441 - ZRA(i)) * (R * Tc(i)) / (Pc(i))) ;
end
V = ((Z * R * T / P) - c);
for i = 1:NC % Loop to calculate average Molar Mass
    MM = MM + x(i)*Mm(i);
end

RHO = MM/V;

else % vapor
V = Z * R * T / P;

for i = 1:NC % Loop to calculate average Molar Mass
    MM = MM + x(i)*Mm(i);
end

RHO = MM/V; %Calculating the density
end
end

```

A.6 Fourth Order Runge-Kutta

The function *RK4* consists of the fourth-order Runge-Kutta solver. The function is called by the function *swirl_func3_deliq* to solve the differential equations for the system in order to find the smallest inlet radius a oil-droplet can have for it to exit through the HPO.

```

function [t,y] = RK4(ODEfile,tspan,yi,h,varargin)
% 4th-order Runge-Kutta

```

```

t=tspan(1):h:tspan(2); %Vector of t-values
if t(end)~=tspan(2)
    t(end+1)=tspan(2);
end

d=diff(t); %Vector of t-increments
yi=(yi(:).')'; % Makes sure it is a column vector

y(:,1)=yi; % Initial condition

for i=1:length(t)-1

    k1 = d(i)*feval(ODEfile,t(i),y(:,i),varargin{:});
    k2 = d(i)*feval(ODEfile,t(i)+d(i)/2,y(:,i)+k1/2,varargin{:});
    k3 = d(i)*feval(ODEfile,t(i)+d(i)/2,y(:,i)+k2/2,varargin{:});
    k4 = d(i)*feval(ODEfile,t(i)+d(i),y(:,i)+k3,varargin{:});

    y(:,i+1) = y(:,i)+(k1+2*k2+2*k3+k4)/6;

end

y=y';
t=t';
end

```

A.7 Shooting Method

The function *shooting_deliq* is called by *swirl_func3_deliq* in order to numerically solve the boundary value problem for the differential equations for the droplet. It uses the Newton-Raphson method to solve the boundary value problems.

```

function [t,y]=shooting_deliq(ODEfile,tspan,h,yf,gamma0,rho,tol,varargin)

% Exactly the same as the shooting function, but just adapted to work for
% the deliquidizer

gammanew=gamma0;
iter=0;
maxiter=100; %100;
fnk=10*yf;
%disp(varargin)

while max(abs(yf-fnk)) > tol && iter<maxiter
    iter=iter+1;
    gammal=gammanew;
    %Specific for swirl_sep2/Swirl_sep2.o: in(6)=rin
    varargin{1}(6)=gammal;
    [t,y]=RK4(ODEfile,tspan,gammal,h,varargin{:});
    fnk=y(end,1);
    if gammal~=0
        dgamma=gammal/100;
    else
        dgamma= 0.01;
    end
    a=gammal+dgamma;

    varargin{1}(6)=a;
    [ta,ya]=RK4(ODEfile,tspan,a,h,varargin{:});
    fnka=ya(end,1);
    jacob=(fnka-fnk)/dgamma;
    a=gammal-dgamma;
    if jacob==0;
        gammanew=gammal+max([abs(dgamma),1.1*tol]);
    else
        gammanew=gammal-rho*inv(jacob)*(fnk-yf);
    end
end

```

```
    end

end

if iter>=maxiter
    disp(['Maximum iterations reached. (rout-Ri)/Ri= ', num2str((fnk-yf)/yf)])
    disp(ODEfile)
end
end
```

B Experimental data

The experimental data obtained from industry and used for comparison against the deliquidizer model are presented in Figures B.1, B.2 and B.3.

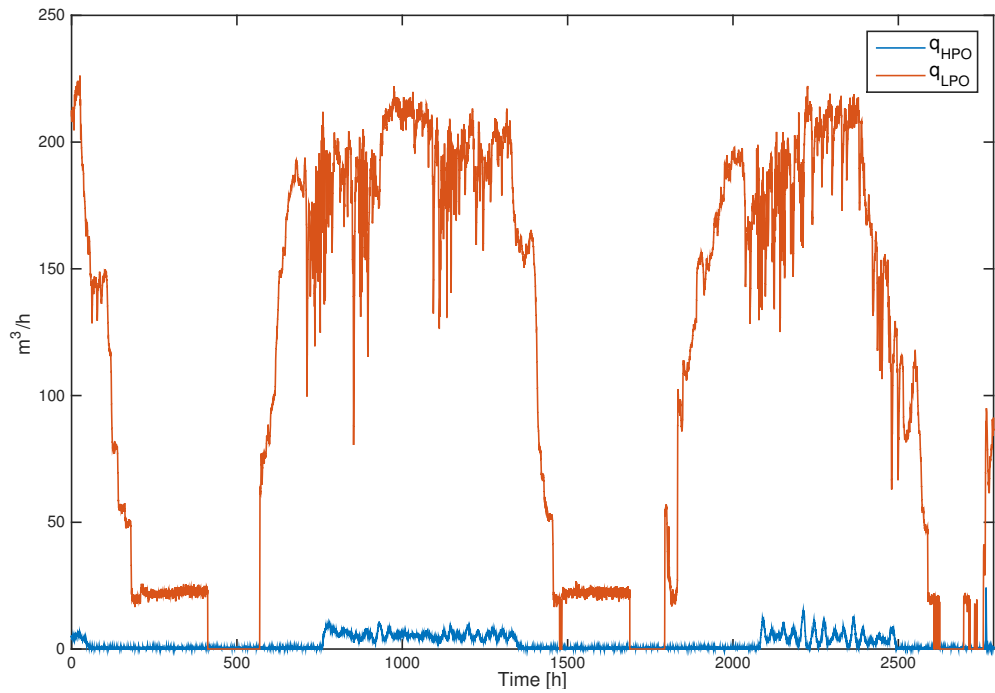


Figure B.1: Time dependent experimental data for the outflows through the light phase outlet (LPO) and the heavy phase outlet (HPO).

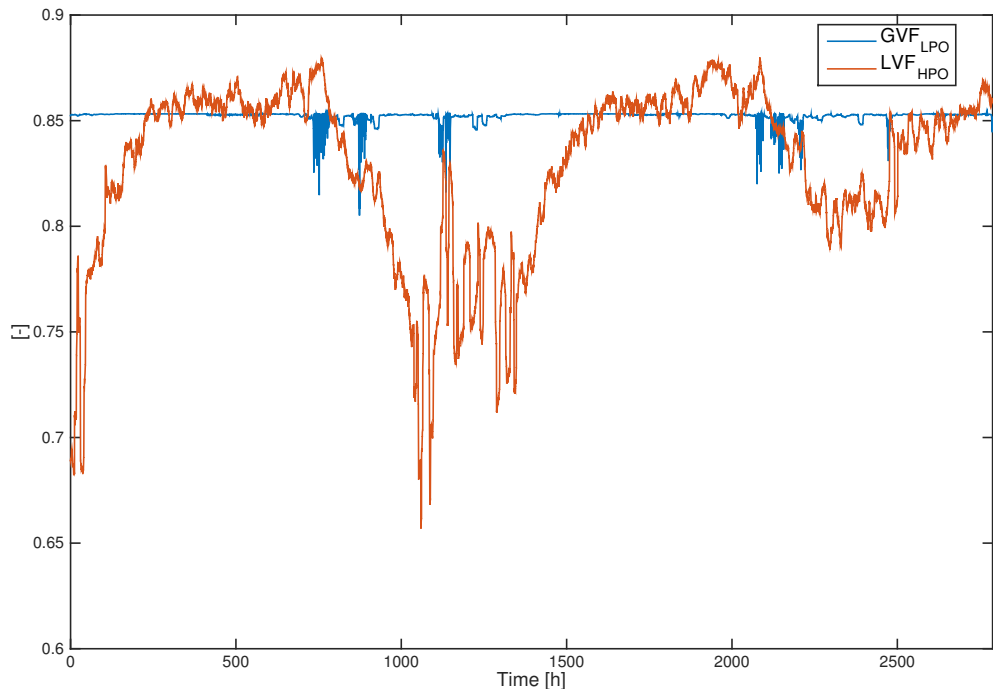


Figure B.2: Time dependent experimental data for the gas volume fraction (GVF) in the light phase outlet (LPO) and liquid volume fraction (LVF) in the heavy phase outlet (HPO) obtained from the industry.

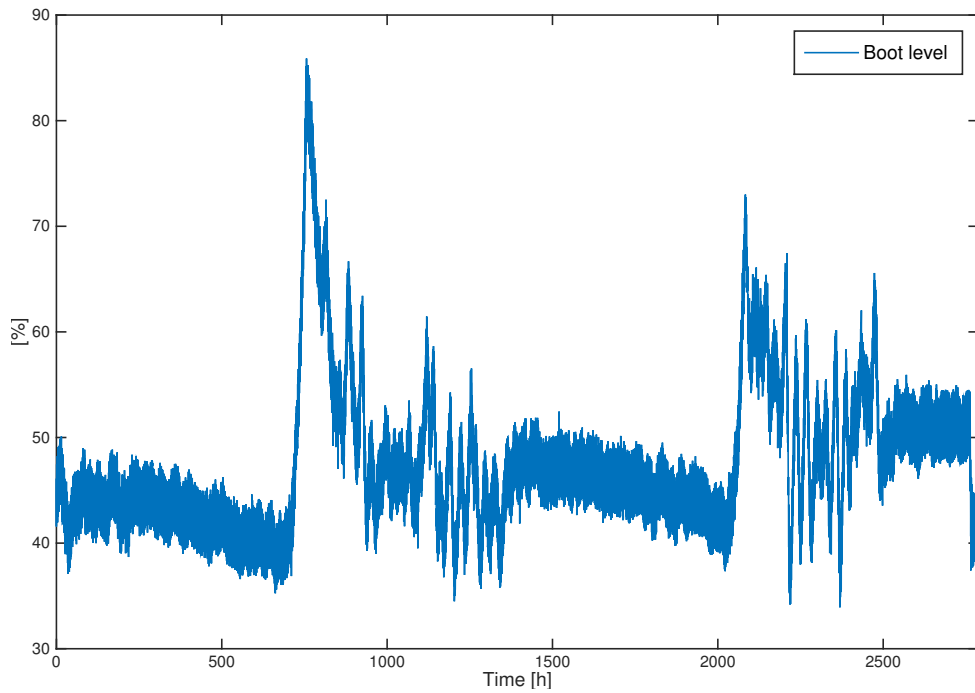


Figure B.3: Data for how much the liquid boot is filled, given in percent, towards the hours of operation.

C Separator profiles

In this appendix the profiles for residence time and droplet size inside the separator as a function of inlet flow, q_{in} , are presented in Figures C.1 and C.2, respectively

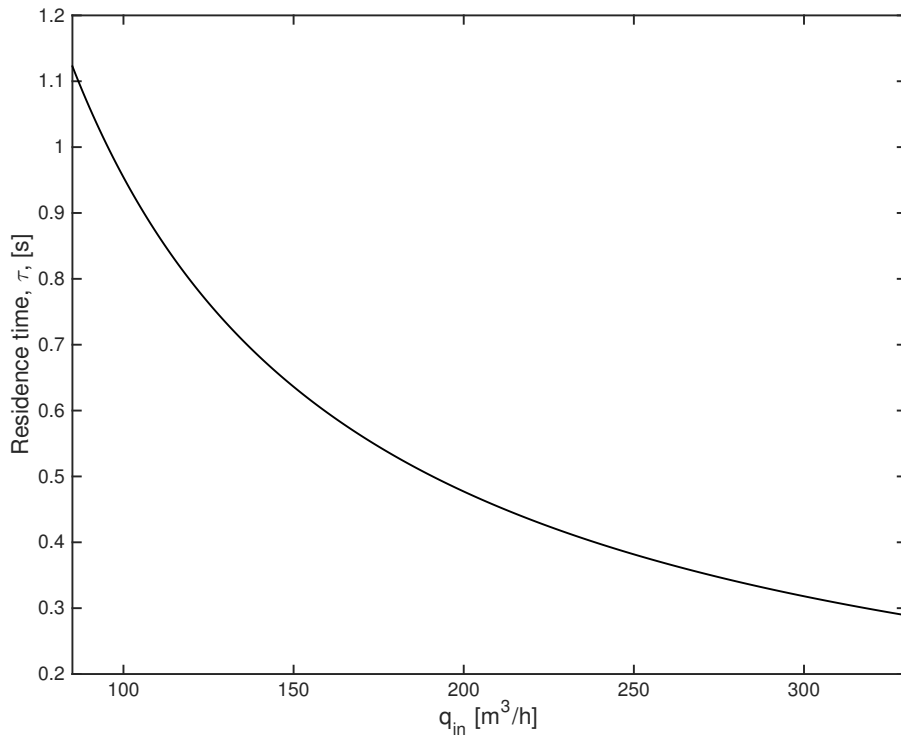


Figure C.1: Residence time in the separator, τ , as a function of inlet flow rate, q_{in} , with a flow split of $FS = 0.8$ and inlet gas fraction of $\alpha_{in} = 0.8$.

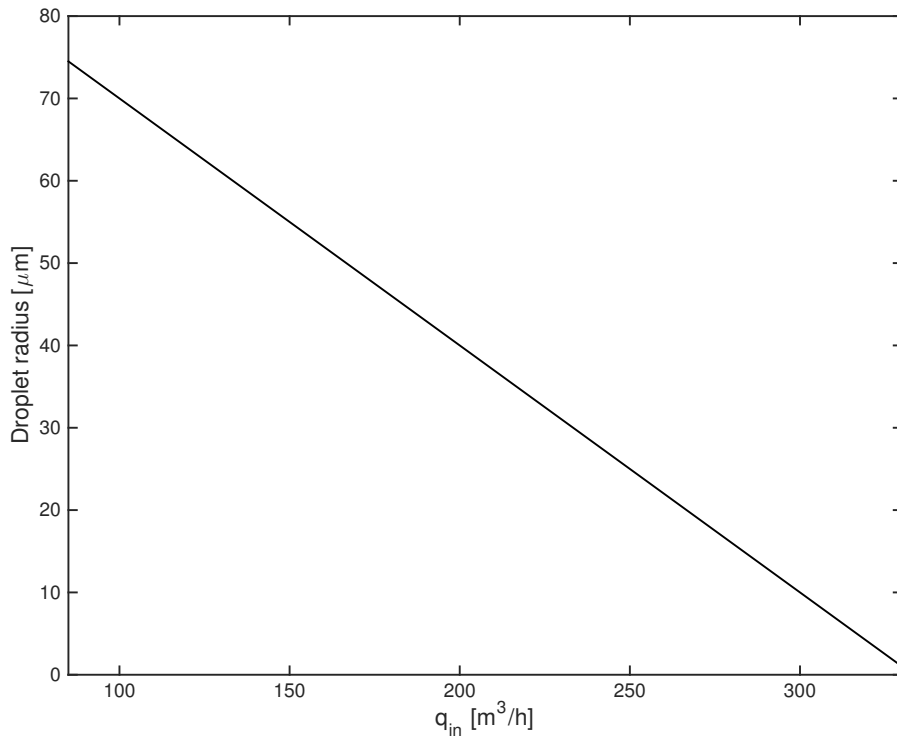


Figure C.2: Droplet size in the separator as a function of inlet flow rate, q_{in} , with a flow split of $FS = 0.8$ and inlet gas fraction of $\alpha_{in} = 0.8$.